L-H Transition in the Mega-Amp Spherical Tokamak

R. J. Akers,[1] G. F. Counsell,[1] A. Sykes,[1] L. C. Appel,[1] E. R. Arends,[1,2] C. Byrom,[1] P. G. Carolan,[1] N. J. Conway,[1]
G. Cunningham,[1] A. Dnestrovskij,[1,3] Yu. N. Dnestrovskij,[1,3] A. R. Field,[1] S. J. Fielding,[1] M. Gryaznevich,[1]
P. Helander,[1] A. Kirk,[1] S. Korsholm,[1,4] R. Martin,[1] H. Meyer,[1] M. P. S. Nightingale,[1] C. M. Roach,[1] V. Shevchenko,[1]
M. Tournianski,[1] M. J. Walsh,[1] C. D. Warrick,[1] The MAST Team,[1] and The NBI Team[1]

[1]*EURATOM/UKAEA Fusion Association, Culham Science Centre, Abingdon, OXON, OX14 3DB, United Kingdom*
[2]*FOM Insituut voor Plasmafysics "Rijnhuizen," Postbus 1207, Nieuwegein, The Netherlands*
[3]*Kurchatov Institute, Institute of Nuclear Fusion, Moscow, Russia*
[4]*Association EURATOM-Risø National Laboratory, Optics and Fluid Dynamics Department, P.O. Box 49, DK-4000 Roskilde,
Denmark*
(Received 21 May 2001; published 3 January 2002)

H-mode plasmas have been achieved on the MAST spherical tokamak at input power considerably higher than predicted by conventional threshold scalings. Following *L-H* transition, a clear improvement in energy confinement is obtained, exceeding recent international scalings even at densities approaching the Greenwald density limit. Transition is accompanied by an order-of-magnitude increase in edge-density gradient, a marked decrease in turbulence, the efficient conversion of internal electron Bernstein waves into free space waves, and the onset and saturation of edge poloidal rotation.

PACS numbers: 52.55.Fa

The first demonstration that the *H*-mode (high confinement) regime was accessible in the spherical tokamak (ST) [1] was provided by the START experiment [2]. Confinement was well represented by *H*-mode scalings [3], even though these scaling laws were developed for conventional aspect-ratio devices. Several factors might have been expected to degrade confinement in START. Vacuum conditions were relatively poor (due to the use of an aluminum tank with viton seals), with correspondingly high radiation losses, and large ion neoclassical transport above moderate density ($n \sim 5 \times 10^{19}$ m^{-3}) was expected to result in significant ion channel losses. Observations of *H*-mode access in the recently commissioned generation of large STs, including the Mega-Amp spherical tokamak (MAST) device [4], are therefore of special interest.

Following boronization in MAST, which produced a tenfold reduction in oxygen and metal impurity radiation, *H*-mode plasmas have been achieved in neutral beam injection (NBI) heated plasmas with modest auxiliary heating power [5,6]. Around 500–700 kW was provided by the NBI system (on loan from ORNL), comparable to the Ohmic heating power. Transition from *L* mode (low confinement) to *H* mode in MAST is clearly demonstrated in the pair of consecutive, nominally identical discharges 2700, 2701 (Fig. 1). The total power input to each shot was $\sim$1.2 MW (0.7 MW Ohmic + 0.52 MW NBI), with NBI termination at 0.25 s (Fig. 1a). Discharge 2701 (shown in gray) remained in *L* mode for the whole discharge; however, shot 2700 underwent *L-H* transition at time 0.22 s as indicated by the sudden reduction in D_α emission (Fig. 1d). Line integral electron density for discharge 2700 increased rapidly following *L-H* transition (Fig. 1b), characteristic of *H*-mode operation, as did the total plasma energy evaluated from magnetic reconstruction (EFIT) (Fig. 1c). Thomson scattering (TS) profiles

taken at time 250 ms in both discharges show that the electron energy, although evaluated just after an edge localized mode (ELM), was $\sim$60% higher in the *H*-mode shot. Similarly, neutral particle analyzer (NPA) data suggest an increase in core ion temperature of $\sim$15% with
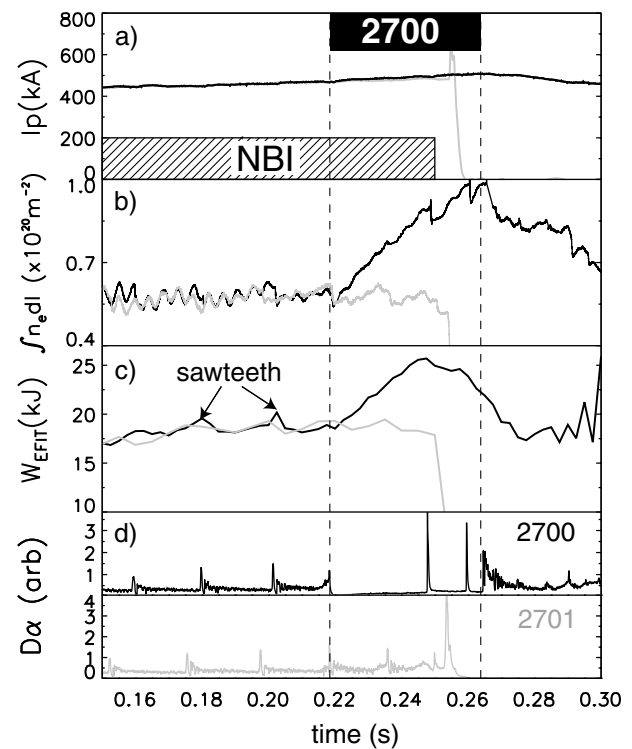
FIG. 1. (a) Plasma current, (b) line integral density from the interferometer, (c) total stored plasma energy, and (d) D_α emission for discharges 2700 (black) and 2701 (gray). Discharge 2700 enters *H* mode at $\sim$220 ms. Dashed lines indicate the *H*-mode phase of discharge 2700.

an ~85% increase in stored thermal ion energy (assuming electron-ion profile similarity and a constant ion dilution $n_{H/D}/n_e = 0.8$ both spatially and temporally).

H-mode power threshold scalings developed for ITER fail to predict the observed threshold for MAST ($P_{th} \sim$ 800 kW), the EPS97 scaling [7] giving ~40 kW with other variants [3] predicting a range from ~10 kW to ~100 kW. This was also the case for START where access to H mode was also achieved only when the total heating power exceeded ~800 kW, compared to the ITER EPS97 prediction of ~9 kW [2]. In contrast, the Canonical Profiles Transport Model (CPTM) [8,9] (which successfully models P_{th} in conventional tokamaks by invoking a critical dimensionless pressure gradient), predicts $P_{th} \sim$ 150 kW for START—much closer to the observed value. Some of the difference may be explained by peripheral charge-exchange losses driven by high-edge neutral densities in START, believed to be of the order 250 kW. Convective losses on MAST, however, are expected to be significantly lower than on START due to lower-edge neutral densities. When applied to density profiles preceding L-H transition for MAST shot 2700, the CPTM model predicts $P_{th} \sim$ 790 kW, very close to the net input power (Ohmic and NBI) of ~750 kW at this time.

Plasma energy evaluated using EFIT has been checked for a wide variety of regimes against that expected from a combination of kinetic measurement (i.e., electron profiles from TS, central ion temperature from NPA) and numerical modeling. Here we have again assumed profile similarity between thermal electrons and ions and an ion dilution $n_{H/D}/n_e = 0.8$ (as was generally the case on START [10]). To evaluate the fast ion stored energy for borderline adiabatic orbits, a newly developed, parallelized version of the LOCUST code [11] has been deployed, where electron drag, thermal ion scattering, and energy diffusion are modeled. Agreement within ~10% between the kinetic and magnetic evaluations is achieved over a wide range of discharge conditions.

For the purpose of calculating the thermal confinement time τ_E for the discharges studied, we have assumed that all of the injected beam power was absorbed, yielding a conservative estimate. Corrections were made for the time derivatives of the stored thermal and magnetic energy and the fast ion stored energy, W_f, but not for plasma expansion and changes to the diamagnetic energy, which are negligible for the quiescent phases of each discharge (i.e., excluding reconnections, disruptions, etc.). Eddy currents induced in the passive conductors (including the center column inconel and graphite limiter) are modeled and, to ensure accurate reconstructions, τ_E has been evaluated only over periods during which the loop voltage remained approximately constant. Figure 2a shows the behavior of the plasma thermal energy for discharge 2928 (where we have subtracted $W_f \sim$ 4.3 kJ, calculated at the TS time of 295 ms). Figure 2b shows the D_α and soft-x-ray (SXR) traces and Fig. 2c the calculated τ_E. The average τ_E over
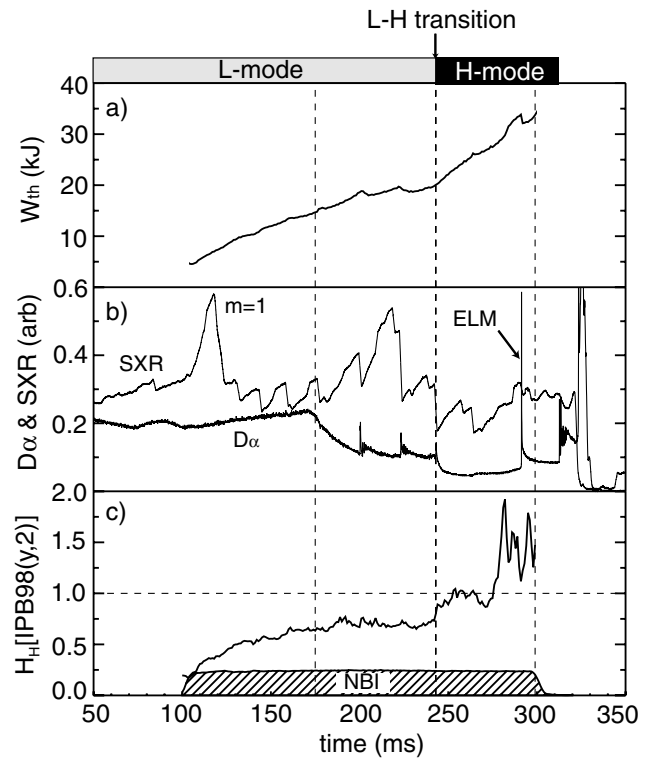
FIG. 2. (a) Thermal plasma energy from EFIT (fast ion subtracted), (b) soft x-ray signal and D_α signal, and (c) H factor [w.r.t. IPB98(y, 2)] for discharge 2928.

the L-mode period (175–243 ms) is ~19 ms and over the H-mode period (243–299 ms), up to the point of NBI termination (including one ELM), is ~45 ms.

Ideal MHD ballooning stability analysis of H-mode discharges 2700 and 2928 at the TS time (assuming that electrons and thermal ions have similar peripheral profiles), indicates that the plasma edge is very close to the ideal ballooning limit. The observed ELMs are thus likely to be type I, although a frequency dependence on injected power during regular ELMing phases has yet to be established. The ELM at ~290 ms in discharge 2928 results in a drop in stored energy of approximately 2 kJ (~4.5% of total). This is typical and is comparable with the ejected energy due to type I ELMs in conventional tokamaks (2%–6%) but is less than the value of ~8% predicted by a scaling law developed at conventional aspect ratio [3].

Figure 3 shows τ_E (averaged over a suitable window) for the plasmas studied against those predicted by ITER ELMy H-mode scaling IPB98(y, 2), together with data from START. For MAST, edge safety factor q_{95} varied between 2.9 and 7.5 for L-mode plasmas and 4.1 and 5.5 for H-mode shots. Greenwald numbers ($= \bar{n}_{e20}\pi a^2/I_p$) for the H-mode plasmas ranged from 0.25 to 0.85, with no evidence of confinement degradation as density increases. The marked improvement in τ_E at transition on MAST is in contrast to results from START, where this was observed only for the highest current discharges [2]. This difference may be due in part to an increase in convective losses on
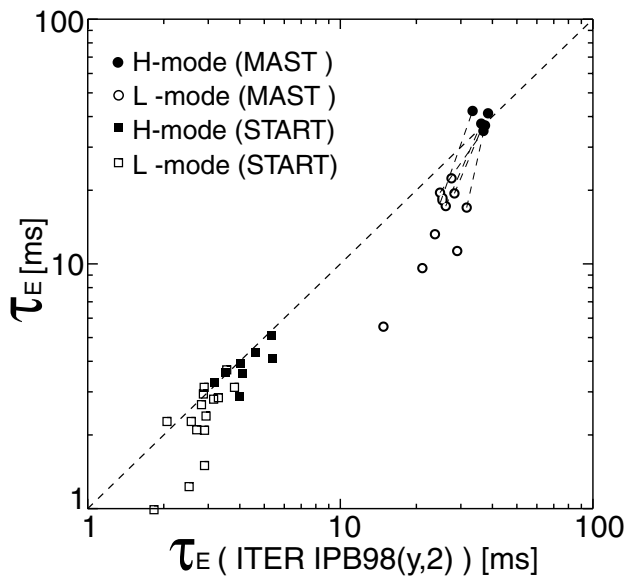
FIG. 3. Comparison between measured thermal confinement time and the IPB98(y, 2) scaling for L- and H-mode MAST and START plasmas.

FIG. 4. Evolution of the thermal electron radial profile vs normalized poloidal flux; (a) is the density, (b) the temperature, and (c) the pressure.

START (a result of high edge neutral densities) with increasing plasma edge density following transition. Dotted lines in Fig. 3 connecting the MAST L to H-mode phases indicate that the increase in confinement is only partially due to an increase in plasma volume and density as the plasma thermal energy increased following transition (radial position feedback control not having been applied). It is clear from Fig. 2 that the increase in τ_E at transition is spontaneous and from Fig. 3 that H-mode data are in good agreement with the IPB98(y, 2) predictions.

Figure 4a shows the significant steepening in the edge electron density profile in ELM-free H-mode periods first reported in [6], in this case for the high-field side of MAST discharge 2952. Density "ears" form at the plasma periphery, evolving over a time scale of ~20 ms. The change in electron temperature (Fig. 4b) is less marked. The pedestal pressure gradient (Fig. 4c) [with respect to (w.r.t.) normalized poloidal flux] remains nearly constant throughout H mode. A simple 1D phenomenological diffusion model suggests that the observed rise in edge density can be explained by a combination of reduced particle diffusivity and the resulting rise in peripheral fueling efficiency [12].

The reduction in D_α emission (Fig. 5a) and high-frequency activity recorded by the MAST homodyne reflectometer (Fig. 5b), show that L-H transition occurs over a period of a few ms. The reflectometer operates at 33 GHz in X mode, with a passband of 50–125 kHz, giving a density cutoff of ~1×10^{19} m^{-3} (marked on Fig. 4). The drop in high-frequency activity probably indicates a decrease in turbulence, since the edge profiles change relatively slowly as demonstrated in Fig. 4 (although the reflectometer density cutoff location does move radially outwards over ~7 ms by ~10% w.r.t. poloidal flux). Edge
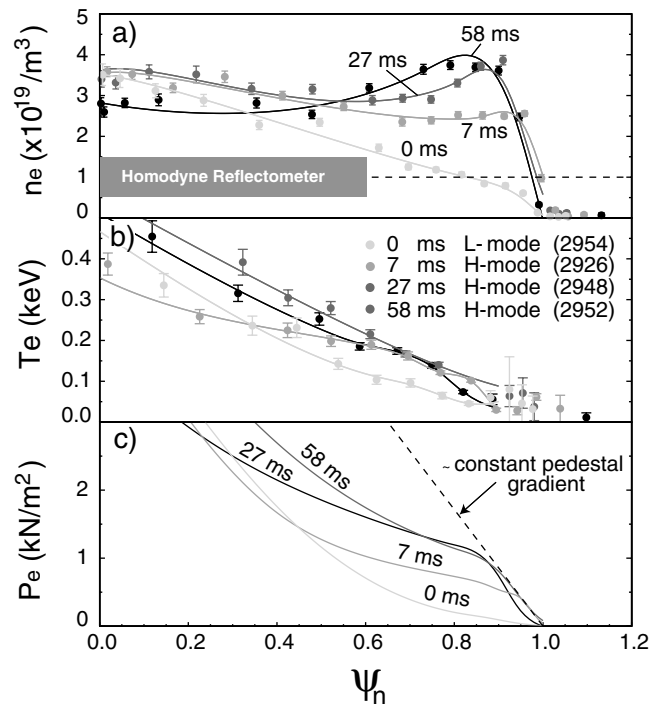
poloidal rotation (Fig. 5c) measured using a peripheral chord of the Doppler spectrometer (C_{III} 464.7 nm, viewing poloidally ~1−2 cm inboard of the last closed flux surface), increases to ~10 km/s (with a corresponding inward-pointing radial electric field). As on START [2] and COMPASS-D [13], rotation onset does not precede the transition.

The observed evolution of edge density and reduction in turbulence between L- and H-mode phases impacts on divertor strike-point characteristics. The L-H transition in shot 2951 is accompanied by an increase in inboard separatrix density from 2 to 4×10^{18} m^{-3} and a rise in electron temperature at the separatrix from ~9 to ~25 eV (measured using Langmuir probes). In addition, a narrowing of the target scrape-off layer temperature width from ~3.5 to ~1 cm is observed, the net result being a strong increase in peak heat flux at the inboard strike point, from ~300 kW m^{-2} to nearly 2.5 MW m^{-2} in H mode. The ratio, R_{oi}, of total power deposited between the outer and inner strike points falls by a factor of ~5, from an average value of ~19.3 in L mode to around 3.6 after transition (very close to the ratio of outboard to inboard separatrix surface areas, which varies from ~3.1 to ~3.5). Data for discharge 2951, together with data from repeat discharge 2952, are shown in Fig. 5. The relative increase in inboard power efflux may result from a reduction in turbulent losses to the outboard side (tentatively inferred from the homodyne reflectometer), whereas the inboard side, which is already at high field and in the good curvature region, may be comparatively unaffected.
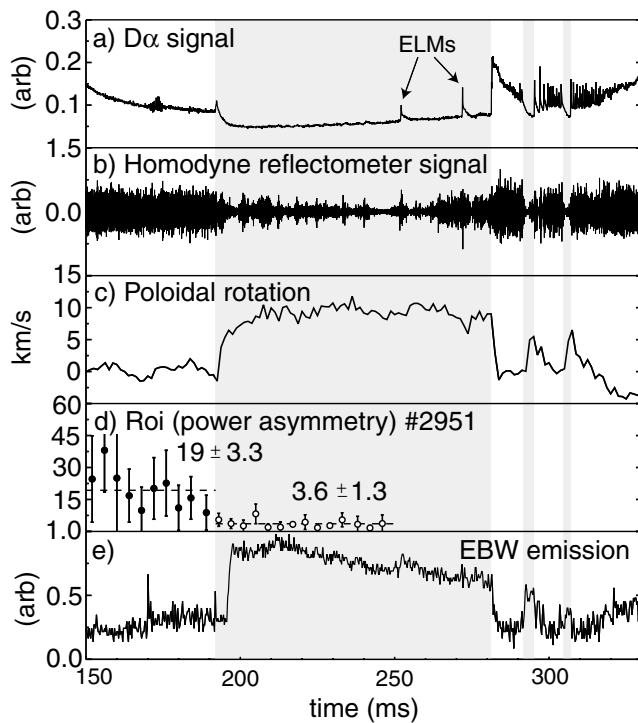
FIG. 5.   (a) D_α emission, (b) midplane homodyne reflectometer signal, (c) poloidal rotation, (d) outboard-inboard power flux asymmetry, and (e) EBW emission during H mode. Plot (d) is for discharge 2951 and plots (a), (b), (c), and (e) are for repeat discharge 2952.

Steepening of the density profile in MAST H mode also impacts on measurements of electron Bernstein wave (EBW) emission from the plasma midplane, taken at an oblique angle close to the optimum for B-X-O mode conversion. In L mode, B-X-O conversion efficiency is close to 100% in the optimal direction but with a narrow angular acceptance cone that only partially overlaps with the receiving antenna. In H mode, the angular window for efficient conversion increases due to the rise in edge density gradient, resulting in full coverage of the antenna pattern by the EBW emission cone and an increase in detected emission up to the thermal level (Fig. 5e). The frequency scanning heterodyne radiometer used for plasma emission measurements was calibrated using X-mode thermal emission from the 2nd EC harmonic at a perpendicular viewing angle and at plasma densities below cutoff, using TS to determine the electron temperature. Near 100% mode conversion with a wide acceptance due to steep edge density gradients, either in H mode or high density L mode, opens up opportunities for using O-X-B mode conversion for ECRF heating and current drive in the spherical tokamak.

In summary, L-H transitions have been achieved on MAST using only $\sim$500 kW of NBI power and H-mode plasmas have been generated with Greenwald numbers up to 0.85. The observed power threshold is significantly higher than that predicted by ITER scalings, but may be explained within the framework of the CPTM model. A substantial increase in particle and energy confinement time is immediately apparent, in contrast to results from START, with thermal energy confinement consistent with that predicted by ITER scalings. Preliminary analysis suggests that the plasma edge is close to the ideal MHD ballooning limit, indicating that ELMs are probably type I. Ejected power due to ELMs is of similar magnitude to that observed for type I ELMs in conventional tokamaks, but less than scalings would suggest. In ELM-free periods, a reduction in turbulence is observed and the edge density increases rapidly, generating a hollow electron density profile on an energy confinement time scale. Following transition, there is a rapid increase and saturation of the edge poloidal flow, and a significant reduction in the outboard-inboard power flux asymmetry across the last closed flux surface, possibly as a result of turbulence suppression. In this regime, the B-X-O mode converted EBW emission cone completely covers the EBW antenna, an encouraging result for the prospect of EBW heating and current drive applications. H mode results from MAST, the first from a new generation of Mega-Amp STs, show promise for the future of the configuration as a burning plasma device, help to shed more light on the physics of the tokamak H mode, and will assist in the development of more robust empirical scalings applicable to all tokamaks.

[1] Y.-K. M. Peng and D. J. Strickler, Nucl. Fusion **26**, 769 (1986).
[2] A. Sykes *et al.*, Phys. Rev. Lett. **84**, 495 (2000).
[3] ITER Physics Basis, Nucl. Fusion **39**, 2232 (1999).
[4] A. C. Darke *et al.*, Fusion Technol. **1**, 799 (1995).
[5] M. Gryaznevich *et al.*, in *Proceedings of the 27th European Physical Society Conference on Controlled Fusion and Plasma Physics, Budapest, 2000* (Institute of Physics Publishing, Bristol, 2000), p. 1705.
[6] A. Sykes *et al.*, Phys. Plasmas **8**, 2101 (2001).
[7] J. A. Snipes, in *Proceedings of the 24th EPS Conference, Berchtesgaden, 1997* (European Physical Society, Geneva, 1997), Pt. III, p. 961.
[8] Yu. Dnestrovskij *et al.*, Plasma Phys. Rep. **26**, 539 (2000).
[9] A. Yu. Dnestrovskij *et al.*, in Ref. [5], p. 1565.
[10] P. G. Carolan, Plasma Phys. Rep. **24**, 206 (1998).
[11] R. J. Akers *et al.*, Nucl. Fusion (to be published).
[12] E. Arends *et al.*, in Proceedings of the 28th EPS Conference on Controlled Fusion and Plasma Physics, Madeira, 2001, P2.028.
[13] R. O'Connell *et al.*, in Ref. [7], p. 1.273.